



Boosting the photovoltaic performance of doctor-bladed organic solar cells using a low-boiling solvent additive

Xue Bai^a, Erming Feng^a, Hengyue Li^a, Jingbo Guo^b, Xiaoming Yuan^a, Huan Liu^a, Qun Luo^b, Yingguo Yang^c, Changqi Ma^b, Chenyi Yi^d, Zijian Zheng^e, Junliang Yang^{a,*}

^a Hunan Key Laboratory for Super-microstructure and Ultrafast Process, School of Physics and Electronics, Central South University, Changsha, 410083, China

^b Printable Electronics Research Center, Suzhou Institute of Nano-Tech and Nano-Bionics, Chinese Academy of Sciences, Suzhou, 215123, China

^c Shanghai Institute of Applied Physics, Chinese Academy of Science, 2019 Jialuo Road, Shanghai, 201800, China

^d Department of Electrical Engineering, Tsinghua University, Beijing, 100084, China

^e Department of Applied Biology and Chemical Technology, Faculty of Science, The Hong Kong Polytechnic University, Hong Kong, China

ARTICLE INFO

Keywords:

Organic solar cells
Low-boiling additive
Doctor-blading
Ambient condition

ABSTRACT

Organic solar cells (OSCs) are attracting much attention due to their distinct benefits of low cost, lightweight and mechanical flexibility. Low-cost and high-throughput approaches combined with large-scale and roll-to-roll (R2R) processes for producing efficient OSCs in ambient condition will considerably speed up the potential commercialization of OSCs. Herein, the low-boiling additive 1,4-difluorobenzene (1,4-DFB) is proposed to produce high-quality PM6:Y6:PC₆₁BM blend active layer dissolved in low-boiling solvent via the doctor blading process in ambient condition. The additive 1,4-DFB can improve the morphology, π - π stacking and phase separation, decrease the charge recombination and produce the red-shift absorption, leading to the enhanced carrier mobility and more balanced charge transport. Thus, it boosts the performance parameters with obviously enhanced short-circuit current and fill factor, and a power conversion efficiency of 15.34% is achieved. Meanwhile, the OSCs with the 1,4-DFB additive treatment also exhibit much better stability. The results demonstrate that low-boiling additive engineering with 1,4-DFB is a powerful route to improve the performance of OSCs prepared by doctor-blading in ambient condition.

1. Introduction

In the past few decades, organic solar cells (OSCs) have attracted extensive attention due to the diversity of synthetic materials, the convenience of fabrication process, and the excellent high flexibility [1–3]. The power conversion efficiency (PCE) of OSCs based on non-fullerene materials has increased year by year [4,5], and it has been increased to over 19% recently and meets the efficiency threshold of photovoltaic marketization [6–8]. In order to realize industrialization, large-scale printing or coating techniques, especially with roll-to-roll (R2R) process, are being developed to fabricate OSCs [9–12].

Additives are widely used to improve the photovoltaic performance of OSCs [13,14]. Xu et al. increased the PCE of layer-by-layer OSC from 13.67% to 15.81% by adding 1 vol% 1-chloronaphthalene (CN) to the PY-IT solution [15]. Ma et al. used binary additives to increase the PCE of layer-by-layer OSCs to 17.8% [16]. Qin et al. created OSCs with a PCE of 18.42% by using 1,4-diiodobenzene (DIB) as a volatile addition,

which remarkably increased molecular crystallization and effectively enhanced the performance of devices [17]. Doctor-blading is a suitable technique for large-scale OSCs production with high repeatability and simplicity of operation. Distler et al. constructed poly[(2,6-(4,8-bis(5-(2-ethylhexyl-3-fluoro)thiophen-2-yl)-benzo[1,2-b:4,5-b'] dithiophene))-alt-(5,5-(1',3'-di-2-thienyl-5',7'-bis(2ethylhexyl)benzo[1',2'-c:4',5'-c']dithiophene-4,8-dione)] (PM6): 2,2'-((2Z,2'Z)-((12,13-bis(2-ethylhexyl)-3,9-diundecyl-12,13-dihydro-[1,2,5]thiadiazolo[3,4-e]thieno[2'',3'':4',5']thieno[2',3':4,5] pyrrolo[3,2-g] thieno[2',3':4,5] thieno[3,2-b]indole-2,10-diyl)bis(methanylylidene))bis(5,6-difluoro-3-oxo-2,3-dihydro-1H-indene-2,1-diylidene))dimalononitrile(Y6): [6,6]-phenyl-C₆₁-butyric acid methyl ester (PC₆₁BM) OSC devices with the area of 26 cm² to get the PCE of 12.6% and enlarged the area to 204 cm² to achieve the PCE of 11.7% using doctor-blading [18]. Ma et al. used PTB7-Th:FOIC:N2200 with 1,8-diiodooctane (DIO) as a solvent additive to prepare p-i-n structure OSCs by the sequential doctor-bladed process and achieved high efficiency of up to 12.27% [19]. Min et al.

* Corresponding author.

E-mail address: junliang.yang@csu.edu.cn (J. Yang).

<https://doi.org/10.1016/j.orgel.2023.106794>

Received 2 December 2022; Received in revised form 28 February 2023; Accepted 17 March 2023

Available online 24 March 2023

1566-1199/© 2023 Elsevier B.V. All rights reserved.

constructed PM6:Y6 OSCs with the PCE of 16.35% utilizing layer-by-layer doctor-blading, which has the advantages such as improved light absorption, adequate vertical phase separation, and practicality [20]. Normally, the active thin film in OSCs would solidify quickly during the spin-coating procedure for high-performance non-fullerene acceptors with high crystallinity and strong aggregation [21–25]. In the case of doctor blading, the wet thin film takes a longer time to be solidified, resulting in a prolonged aggregation and crystallization period in the active layer, leading to the creation of large domains or phase separation. It is why the PCE of spin-coated OSCs is still significantly higher than that of doctor-bladed OSCs [26,27].

Solvent vapor annealing, solvent modification, and high-boiling solvent additives are employed to overcome these difficulties and improve the performance of doctor-bladed active layer films [28–31]. The temperatures of high-boiling solvent additives 1-chloronaphthalene (CN, 260 °C), 1-fluoronaphthalene (FN, 215 °C) and 1,2-diphenoxyethane (DPE, 341 °C) are much higher than those of normally used high-boiling solvents chlorobenzene (CB, 131 °C) and toluene (TL, 110.6 °C), so the drying process of thin film can be redirected to the phase separation [1,25,31–33].

For the fabrication of OSCs with high-boiling solvents, adding high-boiling additives can normally improve doctor-bladed OSCs performance [34]. In the PM6:Y6 system, high-temperature heating is required in the doctor-blading process with high-boiling solvents and high-boiling additives, which would not be helpful for R2R process [29]. Meanwhile, high-boiling additives are difficult to be removed, and their residues have a detrimental influence on the morphology of active layer, lowering the device's efficiency and stability [35].

Because Y6 and its derivatives are extremely sensitive to processing solvent, it performs well in CF solvent [36,37]. For the fabrication of OSCs with low-boiling solvent, the active layer film prepared at ambient temperature often exhibits streaks without solvent additives during the doctor-blading process. Thus, it typically adds high-boiling additive such as CN or DIO during the doctor-blade process. On the one hand, vacuum drying is often required to remove the additives, which would not be helpful for processing large-scale OSCs. On the other hand, it is very difficult to remove the additives completely, leading to excessive aggregate in the active layer and accordingly the performance degradation [18,30]. Thus, high-boiling additives are rarely employed when low-boiling solvent like chloroform (CF) is used in the doctor-blading process [20]. Replacing a high-boiling additive with a low-boiling solvent additive is an effective way to improve spin-coated OSC device performance [38]. As a result, utilizing the low-boiling solvent CF as the host solvent, an effective and easily removed low-boiling additive route to optimize the morphology is necessarily required to improve the PCE of doctor-bladed PM6:Y6 OSCs without vacuum drying.

In this work, high-performance PM6:Y6:PC₆₁BM OSCs are fabricated via doctor blading under ambient conditions by adding a low-boiling additive 1,4-difluorobenzene (1,4-DFB, 88.8 °C) in the active layer solution dissolved in low-boiling solvent CF. The 1,4-DFB-processed PM6:Y6:PC₆₁BM thin film exhibits reasonable small domains and bicontinuous interpenetrating networks, leading to promote charge extraction and limit charge recombination. Thus, doctor-bladed OSCs with 1,4-DFB show a PCE of 15.3% with better short-circuit current (J_{sc}) and fill factor (FF), compared to a PCE of 14.2% for reference OSCs without 1,4-DFB. Furthermore, OSCs fabricated with 1,4-DFB have better stability and could retain more than 90% of its initial efficiency after 55 days of storage in a glove box. The results prove that the performance of doctor-bladed OSC devices can be improved by introducing a low-boiling additive when using a low-boiling host solvent, providing a feasible route for the realization of R2R process of high-performance, large-area OSC devices in ambient conditions.

2. Experimental details

2.1. Materials

PM6, Y6 and PC₆₁BM were purchased from Solarmer Energy Inc. Molybdenum oxide (MoO₃), Ag and CF were purchased from Sigma-Aldrich Inc. The chemicals and solvent were used as received without any further purification. The 1,4-DFB, CN and FN were purchased from Shanghai Titan Technology Co., Ltd. ZnO:PEI composite ink was prepared by the reaction of KOH and Zn(OAc)₂ in methanol solvent, see our previous report for details [39].

2.2. Device fabrication

OSCs were fabricated with an inverted device architecture of ITO/ZnO:PEI/PM6:Y6:PC₆₁BM/MoO₃/Ag. The patterned ITO substrate was cleaned by ultrasonic treatment in deionized water, acetone, and isopropanol for 20 min, respectively. Next, they were dried with pressurized nitrogen before being exposed to a UV-ozone plasma for 25 min. For the active layers, optimized devices were obtained by dissolving PM6, Y6, and PC₆₁BM in CF using a D/A ratio of 1:1.1:0.1, 1:1.1:0.1 with 0.5 vol% 1,4-DFB, 1:1.1:0.1 with 0.5 vol% CN, 1:1.1:0.1 with 0.5 vol% FN, and a total concentration of 20 mg/ml. All solutions were stirred on a hot plate at 40 °C overnight to ensure complete dissolution.

Doctor-blading technique was used to deposit the electron transport layer (ETL) and the active layer in air condition at temperature of 25 °C with a relative humidity of 40%. The gap between the blade and substrate was 300 μm, and the speed of coating was 21 mm/s. The doctor-blading was performed after the dropping of 7 μL ZnO:PEI composite ink at the beginning of the substrate area in ambient condition, leading to an about 25 nm ETL. Subsequently, the doctor-blading was performed after dropping 10 μL PM6:Y6:PC₆₁BM bulk heterojunction (BHJ) solution at the beginning of the substrate area in ambient condition, leading to an about 120 nm BHJ active layer. Then, the deposited thin films were annealed at 100 °C for 10 min in a glovebox. Finally, 10 nm MoO₃ and 100 nm Ag were sequentially deposited as the hole transport layer (HTL) and the anode, respectively, with a mask at the vacuum level of 5×10^{-4} Pa, resulting in an active area of 0.038 cm².

2.3. Characterizations

The current density-voltage (J - V) curves and dark J - V curves of OSCs were measured by a Keithley 2400 unit in air. The AM 1.5G irradiation was provided by a Xenon-lamp-based (Newport 91160S) solar simulator with a light intensity of 100 mW cm⁻² and the light intensity was calibrated by a standard silicon solar cell. An ultraviolet-visible spectrophotometer (Puxi, T9, China) was employed to characterize the absorption of blend thin films and materials. Steady photoluminescence (PL) and the time-resolved photoluminescence (TRPL) measurements of organic blend thin films were performed using a Renishaw system (inVia) under an excitation light of 532 nm. TRPL spectra were monitored at 915 nm. Atomic force microscopy (AFM, Agilent Technologies 5500 AFM/SPM System) and transmission electron microscope (TEM, JEM-2100Plus) were used to characterize the morphology of blend thin films. The crystallographic properties of the active layer were characterized through grazing incidence wide-angle X-ray scattering (GIWAXS). GIWAXS measurements were performed at beamline BL17B1 at Shanghai Synchrotron Radiation Facility. The GIWAXS patterns were obtained with a PILATUS detector of 1475 × 1679 pixels resolution (253.7 mm × 288.18 mm). The 10 keV X-ray beam was incident at a grazing angle of 0.11–0.15°. All characterizations of OSCs were performed under environmental condition without encapsulation.

3. Results and discussion

The polymer PM6 is selected as the donor, non-fullerene small

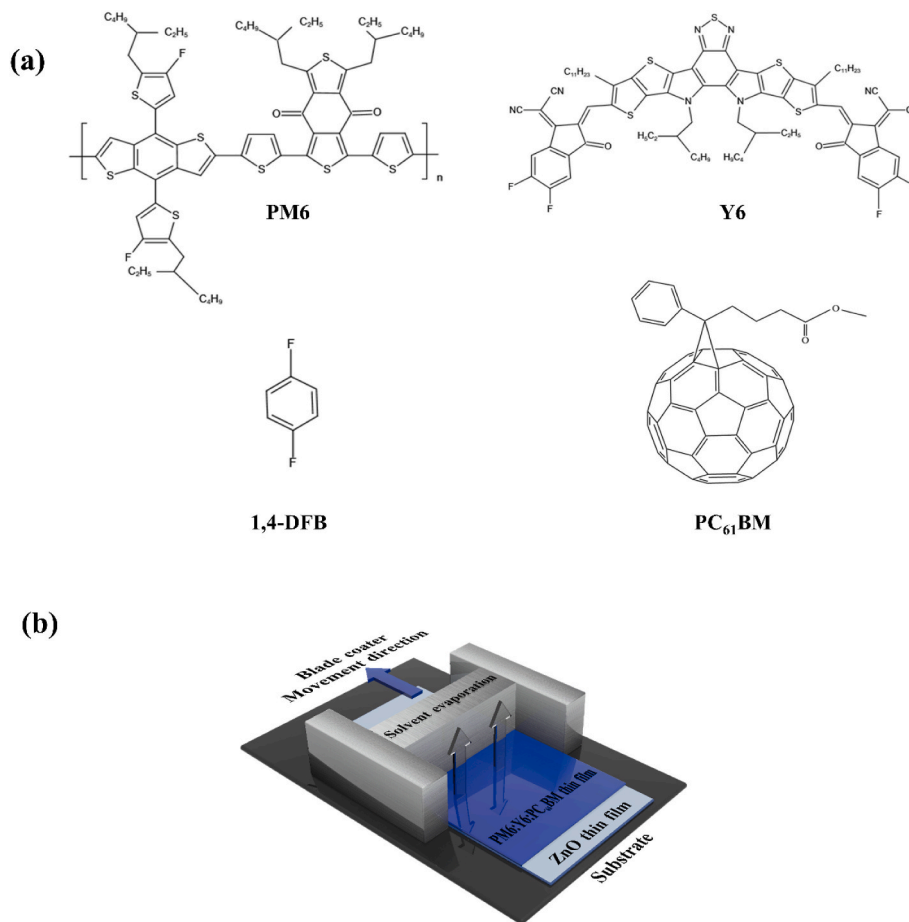


Fig. 1. (a) Chemical structures of PM6, Y6, PC₆₁BM and additive 1,4-DFB. (b) Schematic of doctor-blading process.

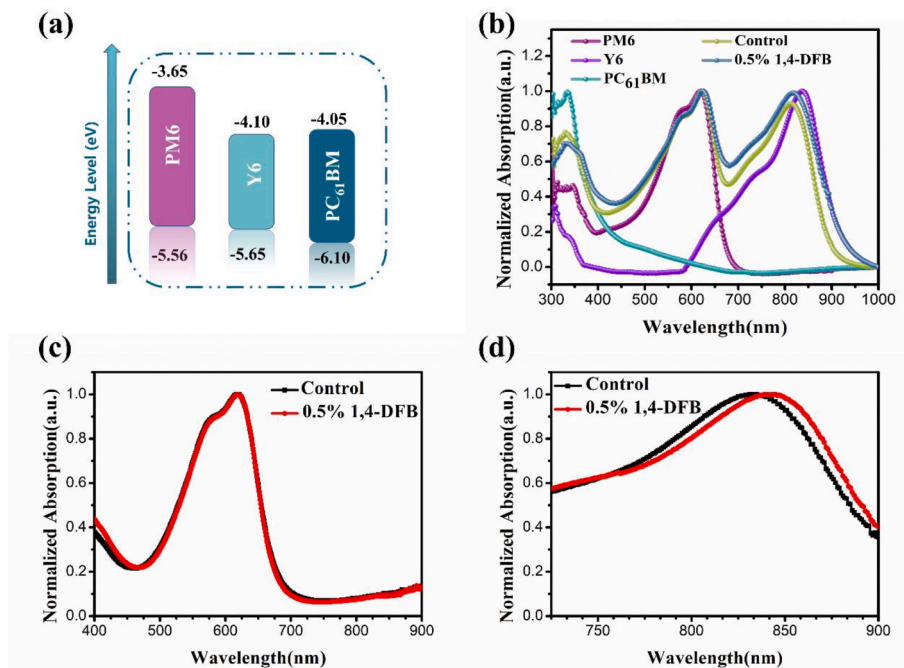


Fig. 2. (a) Energy levels of the donor PM6 and the acceptors Y6 and PC₆₁BM. (b) UV-vis spectra of the doctor-bladed PM6, Y6, PC₆₁BM pure thin films processed without 1,4-DFB and PM6:Y6:PC₆₁BM blend thin films processed with or without 1,4-DFB. (c) UV-vis spectra of the doctor-bladed PM6 pure thin films processed with or without 1,4-DFB. (d) UV-vis spectra of the doctor-bladed Y6 pure thin films processed with or without 1,4-DFB.

Table 1

Photovoltaic parameters of doctor-bladed PM6:Y6:PC₆₁BM OSCs with and without 1,4-DFB additive under simulated AM 1.5G illumination (100 mW cm⁻²). The average PCEs in brackets are obtained from 7 OSC devices.

Additive	PCE (%)	V _{oc} (V)	FF (%)	J _{sc} (mA cm ⁻²)	J _{EQE} (mA cm ⁻²)
Control	14.28 (14.13 ± 0.10)	0.834 (0.829 ± 0.005)	71.4 (72.12 ± 1.2)	23.98 (23.73 ± 0.31)	22.63
0.5% 1,4-DFB	15.34 (15.13 ± 0.12)	0.823 (0.822 ± 0.002)	74.2 (74.47 ± 1.2)	25.12 (24.76 ± 0.42)	24.16

molecules Y6 and PC₆₁BM are selected as the acceptor. The boiling point of 1,4-DFB solvent additive is 88.8 °C. The price and boiling point of some common solvent additives are shown in Table S1. The chemical structures of PM6, Y6, PC₆₁BM and solvent additive 1,4-DFB are shown in Fig. 1a.

Fig. 1b shows a schematic illustration of doctor blading deposition. In order to achieve potentially fully printed OSCs, the ETL ZnO:PEI, the active layer PM6:Y6:PC₆₁BM can be subsequently deposited by doctor blading (Fig. 1b) in ambient condition. The OSCs were fabricated with an inverted device structure of ITO/ZnO:PEI/PM6:Y6:PC₆₁BM/MoO₃/Ag, as shown in Fig. S1a.

As shown in Fig. 2a, the highest occupied molecular orbital (HOMO) level and the lowest unoccupied molecular orbital (LUMO) level of PM6, Y6 and PC₆₁BM are -3.65/-5.56, -5.65/-4.10 and -4.05/-6.01 eV, respectively. The large difference between the HOMO of PM6 and the LUMO of PC₆₁BM is helpful in producing a high open-circuit voltage (V_{oc}) in OSCs. Fig. 2b presents the normalized UV-vis absorbance spectra of the neat thin films of PM6, Y6, and PC₆₁BM, and the blend thin films of PM6:Y6:PC₆₁BM with or without additive. The absorption maxima of the PM6, Y6 and PC₆₁BM thin films are at about 618, 835, and 334 nm, capable of complementary photon absorption. It is found that the 1,4-DFB can enhance the absorption peak of Y6 in the blend thin film, with an obvious red-shift from 820 nm to 835 nm, suggesting that the π-π packing and crystallinity of Y6 may be enhanced [25]. It is discovered that 1,4-DFB primarily affects the Y6 molecule packing,

which in turn influences the packing and morphology of the blend thin film. The normalized absorption spectra of the blend thin film prepared under the different 1,4-DFB concentrations are displayed in Fig. S2. The blend thin film with 0.5% 1,4-DFB shown the strongest absorption spectrum, potentially resulting in a higher J_{sc}.

As shown in Fig. 2c, there is no significant difference in the absorption curves for the PM6 thin films with and without 1,4-DFB. It indicates that 1,4-DFB does not significantly change the molecular packing of PM6 in the thin film due to its high molecular weight. Fig. 2d shows the main absorption peak of the 1,4-DFB-processed Y6 thin film displays a red-shift of 15 nm compared to the pure Y6 thin film. It exhibits the same trend as the blend PM6:Y6:PC₆₁BM thin film processed with the 1,4-DFB additive. The normalized absorption spectra of PM6 and Y6 thin films prepared under the different 1,4-DFB concentrations are displayed in Figs. S3a and S3b. All these indicate that 1,4-DFB can improve intermolecular stacking of the Y6 molecules, which would consequently enhance electron mobility and other electrical properties.

The detailed performance parameters of OSC devices with different fabrication conditions are summarized in Table 1 and Table S2. The control device shows the highest PCE of 14.28% with a V_{oc} of 0.834 V, a J_{sc} of 23.98 mA/cm² and an FF of 71.4%. In contrast, OSC with 0.5% 1,4-DFB additive shows the highest PCE of 15.34% with a V_{oc} of 0.823 V, a J_{sc} of 25.12 mA/cm² and an FF of 74.2%. Fig. 3a and Fig. S4 depict J-V characteristics of the doctor-bladed PM6:Y6:PC₆₁BM BHJ OSCs measured under the illumination of 100 mW cm⁻² (AM 1.5G). Fig. 3b presents the external quantum efficiency (EQE) spectra of OSC devices. The EQE curves of devices are very similar in shape, however, OSC with 1,4-DFB exhibits a stronger photon-to-electron response than the control one in the range of 550–900 nm, which contributes to the enhanced J_{sc}. The EQE maximum of OSC with 1,4-DFB is 84.8%, higher than the control device of 78.9%. The integrated J_{sc} values from the EQE spectra are 22.63 mA/cm² and 24.16 mA/cm² for control and 1,4-DFB-processed OSC devices, respectively, which are consistent with those from the J-V curves. Table S2 and Fig. S4 demonstrate that adding high-boiling additives in the fabrication of OSCs via doctor-blading using low-boiling solvent exhibit poorer performance OSCs, which may result from prolonged drying time and excessive aggregation in the active film.

Furthermore, the long-term storage stability of OSCs in a glove box is

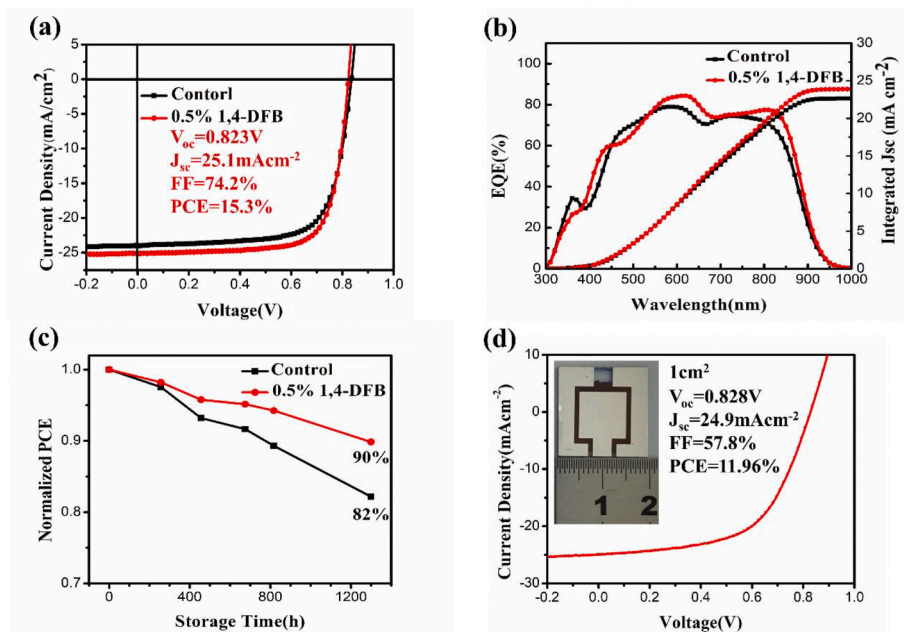


Fig. 3. (a) J-V characteristics of doctor-bladed PM6:Y6:PC₆₁BM BHJ OSCs with and without 1,4-DFB measured under the illumination of 100 mW cm⁻² (AM 1.5G). (b) The corresponding EQE measurements of OSC devices are measured in (a). (c) The changes of PCEs as a function of storage time for OSCs with and without 1,4-DFB. (d) J-V characteristic of 1 cm² OSC devices.

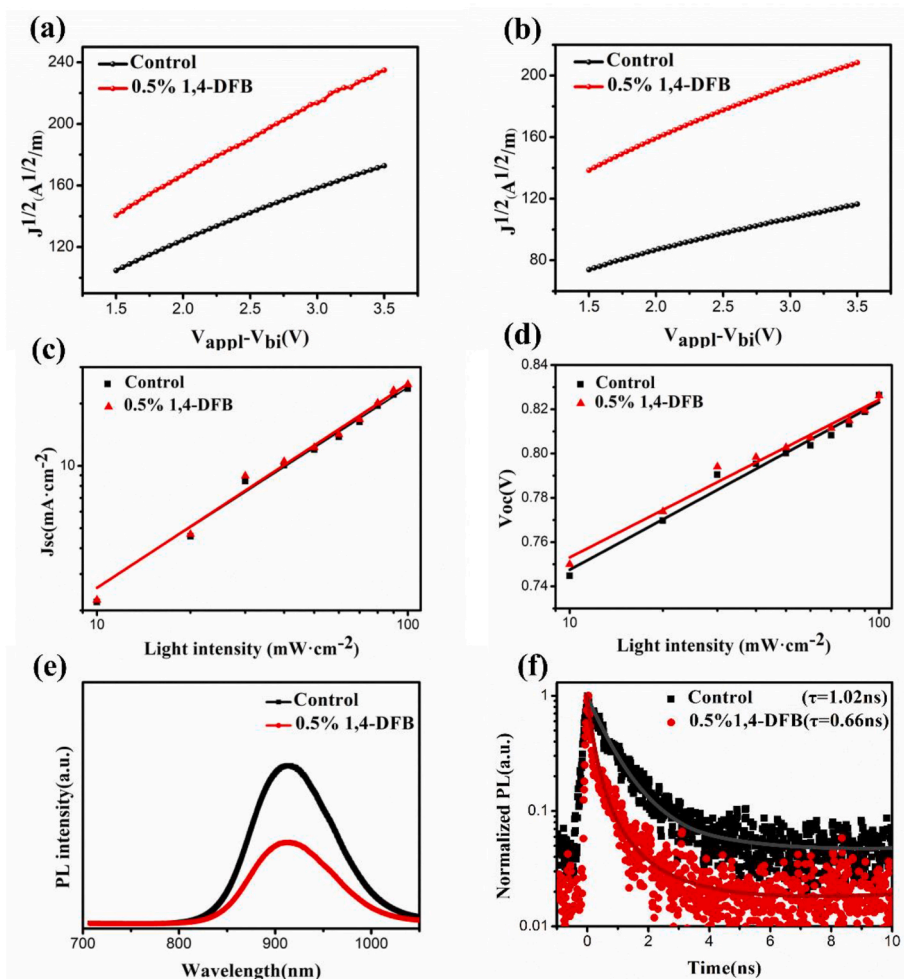


Fig. 4. The dark $J^{1/2}$ - V curves of (a) hole-only and (b) electron-only PM6:Y6:PC₆₁BM devices fabricated with and without 1,4-DFB. (c) V_{oc} and (d) J_{sc} versus the light intensity of doctor-bladed PM6:Y6:PC₆₁BM OSCs processed with and without 1,4-DFB. (e) PL spectra and (f) TRPL spectra of doctor-bladed PM6:Y6:PC₆₁BM blend thin films processed with and without 1,4-DFB.

Table 2

The hole and electron mobilities are measured via SCLC for PM6:Y6:PC₆₁BM blend thin film devices with and without 1,4-DFB.

additive	$\mu_h (\times 10^{-4} \text{ cm}^2 \text{V}^{-1} \text{s}^{-1})$	$\mu_e (\times 10^{-4} \text{ cm}^2 \text{V}^{-1} \text{s}^{-1})$	μ_h/μ_e
Control	3.64	1.12	3.25
0.5% 1,4-DFB	7.08	3.10	2.26

presented in Fig. 3c and Fig. S5. After 1300 h of storage in a nitrogen-filled glove box, the 1,4-DFB-processed and controlled OSC devices maintain the PCEs of 13.77% and 11.76%, exceeding 90% and 82% of their initial values, demonstrating the better stability of OSCs with 1,4-DFB. As the time increases, the BHJ active layer changes to a thermodynamically stable state. The low-boiling additive 1,4-DFB increases molecular ordering of the active layer film, suppresses the donor/acceptor two-phase diffusion and improves the device stability [40]. In addition, a 1,4-DFB-processed large-area device (1.0 cm²) is further fabricated using doctor blading. As shown in Fig. 3d, it exhibits a high PCE of 11.96% with a V_{oc} of 0.828 V, a J_{sc} of 24.9 mA cm⁻², and an FF of 57.8%, indicating the potential application of low-boiling solvent additives in processing the large-area OSCs via printing technology.

Generally speaking, the combined effect of charge transport and charge recombination determines the FF in OSCs. In order to better understand the high FF of OSCs with 1,4-DFB, the space charge limited current (SCLC) is used to measure the charge carrier mobility [36]. The

device configurations of ITO/PEDOT:PSS/active layer/MoO₃/Ag and ITO/ZnO/active layer/PFN-Br/Al are used to measuring the hole mobility and the electron mobility, respectively. The current-voltage ($J^{1/2}$ - V) characteristics are presented in Fig. 4a and b, and the corresponding mobility data are listed in Table 2. For the PM6:Y6:PC₆₁BM blend thin films with 1,4-DFB additive, the hole mobility is enhanced from 3.64×10^{-4} to $7.08 \times 10^{-4} \text{ cm}^2 \text{V}^{-1} \text{s}^{-1}$, and the electron mobility is enhanced from 1.12×10^{-4} to $3.10 \times 10^{-4} \text{ cm}^2 \text{V}^{-1} \text{s}^{-1}$. Furthermore, the hole and electron mobilities of the blend thin film become more balance after the addition of 1,4-DFB. The enhanced carrier mobility and more balanced charge-transfer characteristics are advantageous to the increase FF and the improvement of device performance.

In addition, it is necessary to understand the exciton recombination and recombination dynamics in OSC devices. The changes of J_{sc} and V_{oc} under the different light intensities (P_{light}) are analyzed. The P_{light} dependence of J_{sc} reflects the extent of exciton recombination in devices [41,42]. The relationship between J_{sc} and P_{light} is $J_{sc} \propto P_{light}^\alpha$, where α is an exponential factor. The closer the α is to 1.00, the weaker the bimolecular recombination in the device. From fitting the data of J_{sc} versus P_{light} as illustrated in Fig. 4c, the values of 0.968, 0.985 are obtained for control and 1,4-DFB-processed OSC devices, respectively, which indicates that the addition of 1,4-DFB can effectively suppress bimolecular recombination.

Another loss mechanism is an additional trap-assisted recombination mechanism, the P_{light} dependence of V_{oc} is worth discussing [43,44]. The

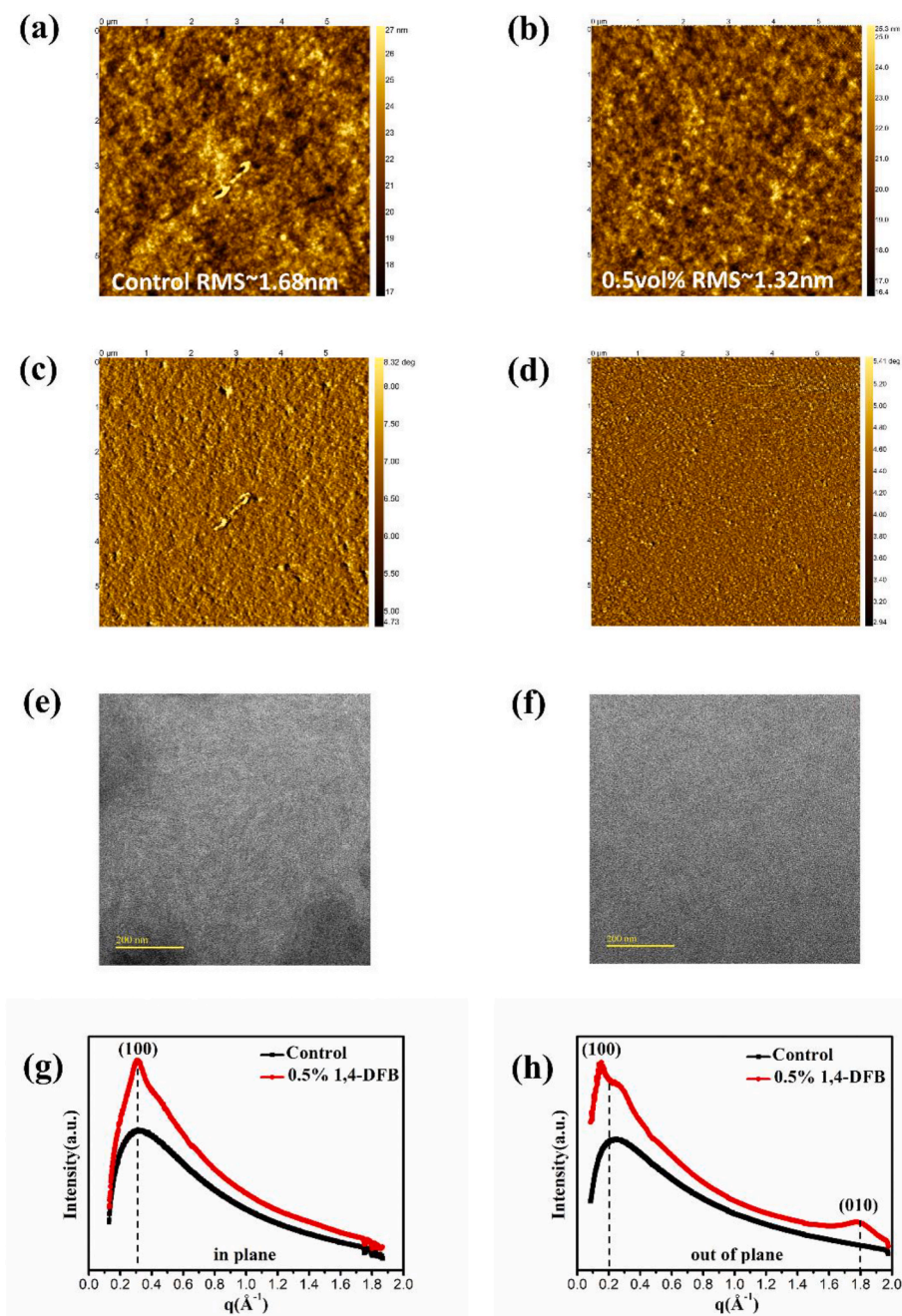


Fig. 5. (a–b) AFM height images of doctor-bladed PM6:Y6:PC₆₁BM OSCs processed with and without 1,4-DFB. (c–d) AFM phase images of doctor-bladed PM6:Y6:PC₆₁BM OSCs processed with and without 1,4-DFB. (e–f) TEM images of doctor-bladed PM6:Y6:PC₆₁BM OSCs processed with and without 1,4-DFB. (g–h) The in-plane and out-of-plane integrated curves of the GIWAXS patterns (showed in Fig. S7) of doctor-bladed PM6:Y6:PC₆₁BM thin films with and without 1,4-DFB.

equation between V_{oc} and P_{light} could be described as $V_{oc} \propto nKT/q \ln(P_{light})$, where K is the Boltzmann constant, T is kelvin temperature, and q is the elementary charge. If n is close to 1, the mechanism is dominated by bimolecular recombination in the active layer [45]. Alternatively, if n is close to 2, the mechanism is dominated by trap-assisted reorganization. As seen from Fig. 4d, the slopes of both control ($n = 1.27$) and 1,4-DFB-processed ($n = 1.20$) OSC devices are close to 1, indicating that bimolecular recombination is dominant in the active layer. When n is greater than 1, trap-assisted or single-molecule recombination in the device is effectively suppressed, and higher values of n indicate stronger trap-assisted or monomolecular recombination. The slope of OSCs with 1,4-DFB is a little smaller than the control one, indicating reduced trap-assisted recombination. The decrease in bimolecular recombination

and trap-assisted recombination should be responsible for the increase in J_{sc} and FF .

In order to examine the charge dynamics of OSCs, the PL and TRPL of PM6:Y6:PC₆₁BM thin films are measured [46,47]. As shown in Fig. 4e, the control sample shows a strong PL emission, and the emission peak at approximately 915 nm. The PL spectra of the blend films with different concentrations of 1,4-DFB as additive are shown in Fig. S6. The PL emission is significantly quenched for the sample with 1,4-DFB, suggesting that the donor/acceptor interface for exciton dissociation is increasingly larger, which is more favorable for exciton dissociation and charge separation.

Furthermore, TRPL spectroscopy can be used to show how fast the quenching process occurs for a better understanding the exciton

transport and dissociation. Fig. 4f shows the carrier lifetimes of two samples calculated by fitting the PL decay curves with a conventional bi-exponential model. Table S3 summarizes the TRPL parameters under the different 1,4-DFB concentrations. The control sample has a carrier lifetime of 1.61 ns. While the sample with 1,4-DFB has a carrier lifetime of 0.74 ns, which exhibits a lower carrier lifetime than the control one. The results reveal that the sample with 1,4-DFB has better charge transfer efficiency from the donor domain to the acceptor domain, as well as more efficient exciton dissociation, both of which are beneficial for photocurrent generation.

AFM and TEM are used to investigate the surface morphology and phase separation of PM6:Y6:PC₆₁BM blend thin films processed by doctor-blading in ambient condition with or without additive. As shown in Fig. 5a and b, the root-mean-square (RMS) roughnesses of the AFM height image surfaces are 1.68 nm and 1.32 nm for the control and 1,4-DFB-processed blend thin film, respectively. As shown in Fig. 5c and d the AFM phase images show that a more flat and dense active layer film is prepared by adding 1,4-DFB, which is conducive to the formation of good contact between the ZnO and the active layer, as well as the MoO₃ and the active layer, resulting in a higher FF. The surface of blend thin film without 1,4-DFB contains aggregates, which are not conducive to exciton dissociation and charge transport, thus, to some degree, limiting J_{sc} and FF. As shown in Fig. 5e and f, the bright and dark domains correspond to the domains rich in donors and acceptors, respectively. The phase separation between the white and dark domains becomes more contracted with 1,4-DFB, indicating improved phase separation.

The results discussed above can be further verified by two-dimensional (2D) GIWAXS characterization. The GIWAXS patterns and their corresponding out-of-plane and in-plane integrated curves of PM6:Y6:PC₆₁BM thin films fabricated by doctor-blading in ambient condition are shown in Figs. S7a–b and Fig. 5g and h, respectively. Both blend thin films show a distinct (100) lamellar stacking peak in the in-plane direction at the same position at $q = 0.30 \text{ \AA}^{-1}$ (Fig. 5g). Compared with the blend thin film without additive, the peak strength of the blend thin film with 1,4-DFB is significantly enhanced. In the out-of-plane direction, the same (100) lamellar stacking peak at $q = 0.30 \text{ \AA}^{-1}$ can also be observed (Fig. 5h), and the intensity variation trend is the same as that of the in-plane diffraction peak. Notably, a typical π - π diffraction peak belonging to the acceptor Y6 located at $q_z = 1.77 \text{ \AA}^{-1}$ in the out-of-plane direction can be obviously observed for the blend thin film with 1,4-DFB, which is absent in reference sample. It explains the red-shift of the absorption peak of the acceptor Y6 in Fig. 2d. The result suggests that the additive 1,4-DFB can greatly improve the crystallinity of PM6:Y6:PC₆₁BM blend thin film and the enhanced π - π stacking, leading to better charge transport and higher J_{sc} and FF.

4. Conclusions

In summary, we report that a simple structure, low-boiling solvent additive 1,4-DFB can promote the PCEs of PM6:Y6:PC₆₁BM OSCs increase from 14.28% to 15.34% fabricated with doctor-blading in ambient conditions. The addition of 1,4-DFB additive is helpful to form high-quality PM6:Y6:PC₆₁BM blend thin film and high-performance OSCs for several reasons: (i) improving nanostructure and supporting forming a bicontinuous interpenetrating networks; (ii) increasing carrier mobility and producing more balanced charge transfer characteristics; (iii) more effective inhibition of bimolecular recombination with reduced trap-assisted recombination. Furthermore, 1,4-DFB as a low-boiling solvent additive can improve the photovoltaic performance of doctor-bladed OSCs with non-fullerene acceptor systems using low-boiling solvents. It provides a good route for exploring the potential industrial application of large-area high-efficiency and stable OSCs.

Declaration of competing interest

The authors declare that they have no known competing financial interests or personal relationships that could have appeared to influence the work reported in this paper.

Data availability

Data will be made available on request.

Acknowledgements

This work is supported by the National Key Research and Development Program of China (2022YFB3803300), the National Natural Science Foundation of China (51673214, 61974166). X.B. also thanks the support from the Fundamental Research Funds for the Central Universities of Central South University (Grant No. 2021zzts0495). The authors also thank the BL17B1 and BL19U beamlines in Shanghai Synchrotron Radiation Facility for GIWAXS experiments and User Experimental Assist System of SSRF.

Appendix B. Supplementary data

Supplementary data to this article can be found online at <https://doi.org/10.1016/j.orgel.2023.106794>.

References

- [1] Y. Zheng, T. Goh, P. Fan, W. Shi, J. Yu, A.D. Taylor, Toward efficient thick active PTB7 photovoltaic layers using diphenyl ether as a solvent additive, *ACS Appl. Mater. Interfaces* 8 (2016) 15724–15731.
- [2] L. Dou, J. You, Z. Hong, Z. Xu, G. Li, R.A. Street, Y. Yang, 25th anniversary article: a decade of organic/polymeric photovoltaic research, *Adv. Mater.* 25 (2013) 6642–6671.
- [3] F. Qin, L. Sun, H. Chen, Y. Liu, X. Lu, W. Wang, T. Liu, X. Dong, P. Jiang, Y. Jiang, 54 cm² large-area flexible organic solar modules with efficiency above 13, *Adv. Mater.* 33 (2021), 2103017.
- [4] Y. Cui, Y. Xu, H. Yao, P. Bi, L. Hong, J. Zhang, Y. Zu, T. Zhang, J. Qin, J. Ren, Single-junction organic photovoltaic cell with 19% efficiency, *Adv. Mater.* 33 (2021), 2102420.
- [5] W. Li, L. Ye, S. Li, H. Yao, H. Ade, J. Hou, A high-efficiency organic solar cell enabled by the strong intramolecular electron push–pull effect of the nonfullerene acceptor, *Adv. Mater.* 30 (2018), 1707170.
- [6] N. Yeh, P. Yeh, Organic solar cells: their developments and potentials, *Renew. Sustain. Energy Rev.* 21 (2013) 421–431.
- [7] C.J. Brabec, Organic photovoltaics: technology and market, *Sol. Energy Mater. Sol. Cell.* 83 (2004) 273–292.
- [8] L. Zhu, M. Zhang, J. Xu, C. Li, J. Yan, G. Zhou, W. Zhong, T. Hao, J. Song, X. Xue, Single-junction organic solar cells with over 19% efficiency enabled by a refined double-fibril network morphology, *Nat. Mater.* 21 (2022) 656–663.
- [9] J. Wei, C. Zhang, G. Ji, Y. Han, I. Ismail, H. Li, Q. Luo, J. Yang, C.-Q. Ma, Roll-to-roll printed stable and thickness-independent ZnO: PEI composite electron transport layer for inverted organic solar cells, *Sol. Energy* 193 (2019) 102–110.
- [10] L. Yang, S. Tong, C. Gong, H. Xia, C. Wang, B. Liu, H. Xie, S. Xiao, J. He, Large-scale roll-to-roll micro-gravure printed flexible PBDB-T/IT-M bulk heterojunction photodetectors, *Appl. Phys. A* 126 (2020) 1–9.
- [11] X. Guo, H. Li, Y. Han, Y. Yang, Q. Luo, C.-Q. Ma, J. Yang, Fully doctor-bladed efficient organic solar cells processed under ambient condition, *Org. Electron.* 82 (2020), 105725.
- [12] H. Li, C. Zhang, J. Wei, K. Huang, X. Guo, Y. Yang, S. So, Q. Luo, C.-Q. Ma, J. Yang, Roll-to-roll micro-gravure printed P3HT: PCBM organic solar cells, *Flex. Print. Electron.* 4 (2019), 044007.
- [13] C. McDowell, M. Abdelsamie, M.F. Toney, G.C. Bazan, Solvent additives: key morphology-directing agents for solution-processed organic solar cells, *Adv. Mater.* 30 (2018), 1707114.
- [14] L. Liu, Y. Kan, K. Gao, J. Wang, M. Zhao, H. Chen, C. Zhao, T. Jiu, A.-K.Y. Jen, Y. Li, Graphdiyne derivative as multifunctional solid additive in binary organic solar cells with 17.3% efficiency and high reproductivity, *Adv. Mater.* 32 (2020), 1907604.
- [15] W. Xu, X. Zhu, X. Ma, H. Zhou, X. Li, S.Y. Jeong, H.Y. Woo, Z. Zhou, Q. Sun, F. Zhang, Achieving 15.81% and 15.29% efficiency of all-polymer solar cells based on layer-by-layer or bulk heterojunction structure, *J. Mater. Chem.* 10 (2022) 13492–13499.
- [16] X. Ma, Q. Jiang, W. Xu, C. Xu, S.Y. Jeong, H.Y. Woo, Q. Wu, X. Zhang, G. Yuan, F. Zhang, Layered optimization strategy enables over 17.8% efficiency of layer-by-layer organic photovoltaics, *Chem. Eng. J.* 442 (2022), 136368.

- [17] J.Q. Qin, Q.G. Yang, J. Oh, S.S. Chen, G.O. Odunmbaku, N.A.N. Ouedraogo, C. Yang, K. Sun, S.R. Lu, Volatile solid additive-assisted sequential deposition enables 18.42% efficiency in organic solar cells, *Adv. Sci.* 9 (2022), 2105347.
- [18] A. Distler, C.J. Brabec, H.J. Egelhaaf, Organic photovoltaic modules with new world record efficiencies, *Prog. Photovoltaics Res. Appl.* 29 (2021) 24–31.
- [19] Y. Wang, Q. Zhu, H.B. Naveed, H. Zhao, K. Zhou, W. Ma, Sequential blade-coated acceptor and donor enables simultaneous enhancement of efficiency, stability, and mechanical properties for organic solar cells, *Adv. Energy Mater.* 10 (2020), 1903609.
- [20] R. Sun, Q. Wu, J. Guo, T. Wang, Y. Wu, B. Qiu, Z. Luo, W. Yang, Z. Hu, J. Guo, A layer-by-layer architecture for printable organic solar cells overcoming the scaling lag of module efficiency, *Joule* 4 (2020) 407–419.
- [21] F. Bai, J. Zhang, A. Zeng, H. Zhao, K. Duan, H. Yu, K. Cheng, G. Chai, Y. Chen, J. Liang, A highly crystalline non-fullerene acceptor enabling efficient indoor organic photovoltaics with high EQE and fill factor, *Joule* 5 (2021) 1231–1245.
- [22] Y. Liu, Y. Yan, Q. Zhang, J. Zhang, X. Yu, Y. Han, Increasing the nucleation and growth barrier of a non-fullerene acceptor to achieve bicontinuous pathways in semitransparent ternary polymer solar cells, *J. Mater. Chem. C* 9 (2021) 5713–5722.
- [23] L. Perdigón-Toro, H. Zhang, A. Markina, J. Yuan, S.M. Hosseini, C.M. Wolff, G. Zuo, M. Stollerfoht, Y. Zou, F. Gao, Barrierless free charge generation in the high-performance PM6: Y6 bulk heterojunction non-fullerene solar cell, *Adv. Mater.* 32 (2020), 1906763.
- [24] X. Xu, L. Yu, H. Yan, R. Li, Q. Peng, Highly efficient non-fullerene organic solar cells enabled by a delayed processing method using a non-halogenated solvent, *Energy Environ. Sci.* 13 (2020) 4381–4388.
- [25] Q. Li, L.-M. Wang, S. Liu, L. Guo, S. Dong, G. Ma, Z. Cao, X. Zhan, X. Gu, T. Zhu, Vertical composition distribution and crystallinity regulations enable high-performance polymer solar cells with > 17% efficiency, *ACS Energy Lett.* 5 (2020) 3637–3646.
- [26] Y. Yang, E. Feng, H. Li, Z. Shen, W. Liu, J. Guo, Q. Luo, J. Zhang, G. Lu, C. Ma, Layer-by-layer slot-die coated high-efficiency organic solar cells processed using twin boiling point solvents under ambient condition, *Nano Res.* 14 (2021) 4236–4242.
- [27] H. Li, K. Huang, Y. Dong, X. Guo, Y. Yang, Q. Luo, C.-Q. Ma, D. Li, G. Lu, J. Xiong, J. Zhang, Y. Yang, X. Gao, J. Yang, Efficient organic solar cells with the active layer fabricated from glovebox to ambient condition, *Appl. Phys. Lett.* 117 (2020), 133301.
- [28] Y. Lin, L. Yu, Y. Xia, Y. Firdaus, S. Dong, C. Müller, O. Inganäs, F. Huang, T. D. Anthopoulos, F. Zhang, One-step blade-coated highly efficient nonfullerene organic solar cells with a self-assembled interfacial layer enabled by solvent vapor annealing, *Solar RRL* 3 (2019), 1900179.
- [29] Y. Li, H. Liu, J. Wu, H. Tang, H. Wang, Q. Yang, Y. Fu, Z. Xie, Additive and high-temperature processing boost the photovoltaic performance of nonfullerene organic solar cells fabricated with blade coating and nonhalogenated solvents, *ACS Appl. Mater. Interfaces* 13 (2021) 10239–10248.
- [30] Y. Yu, R. Sun, T. Wang, X. Yuan, Y. Wu, Q. Wu, M. Shi, W. Yang, X. Jiao, J. Min, Improving photovoltaic performance of non-fullerene polymer solar cells enables by fine-tuning blend microstructure via binary solvent mixtures, *Adv. Funct. Mater.* 31 (2021), 2008767.
- [31] J. Lv, H. Tang, J. Huang, C. Yan, K. Liu, Q. Yang, D. Hu, R. Singh, J. Lee, S. Lu, Additive-induced miscibility regulation and hierarchical morphology enable 17.5% binary organic solar cells, *Energy Environ. Sci.* 14 (2021) 3044–3052.
- [32] L. Ye, Y. Xiong, M. Zhang, X. Guo, H. Guan, Y. Zou, H. Ade, Enhanced efficiency in nonfullerene organic solar cells by tuning molecular order and domain characteristics, *Nano Energy* 77 (2020), 105310.
- [33] Q. Wu, D. Zhao, A.M. Schneider, W. Chen, L. Yu, Covalently bound clusters of alpha-substituted PDI rival electron acceptors to fullerene for organic solar cells, *J. Am. Chem. Soc.* 138 (2016) 7248–7251.
- [34] Y.W. Han, H.S. Lee, D.K. Moon, Printable and semitransparent nonfullerene organic solar modules over 30 cm² introducing an energy-level controllable hole transport layer, *ACS Appl. Mater. Interfaces* 13 (2021) 19085–19098.
- [35] L. Ye, Y. Jing, X. Guo, H. Sun, S. Zhang, M. Zhang, L. Huo, J. Hou, Remove the residual additives toward enhanced efficiency with higher reproducibility in polymer solar cells, *J. Phys. Chem. C* 117 (2013) 14920–14928.
- [36] J. Yuan, Y. Zhang, L. Zhou, G. Zhang, H.-L. Yip, T.-K. Lau, X. Lu, C. Zhu, H. Peng, P. A. Johnson, Single-junction organic solar cell with over 15% efficiency using fused-ring acceptor with electron-deficient core, *Joule* 3 (2019) 1140–1151.
- [37] K. Jiang, Q. Wei, J.Y.L. Lai, Z. Peng, H.K. Kim, J. Yuan, L. Ye, H. Ade, Y. Zou, H. Yan, Alkyl chain tuning of small molecule acceptors for efficient organic solar cells, *Joule* 3 (2019) 3020–3033.
- [38] J. Chen, F. Pan, Y. Cao, J. Chen, Low boiling point solvent additives enable vacuum drying-free processed 230 nm thick PTB7-Th: PC₇₁BM active layers with more than 10% power conversion efficiency, *J. Mater. Chem.* 7 (2019) 1861–1869.
- [39] N. Wu, Q. Luo, Z. Bao, J. Lin, Y.-Q. Li, C.-Q. Ma, Zinc oxide: conjugated polymer nanocomposite as cathode buffer layer for solution processed inverted organic solar cells, *Sol. Energy Mater. Sol. Cells* 141 (2015) 248–259.
- [40] Q. He, W. Sheng, M. Zhang, G. Xu, P. Zhu, H. Zhang, Z. Yao, F. Gao, F. Liu, X. Liao, Revealing morphology evolution in highly efficient bulk heterojunction and pseudo-planar heterojunction solar cells by additives treatment, *Adv. Energy Mater.* 11 (2021), 2003390.
- [41] T. Liu, Z. Luo, Y. Chen, T. Yang, Y. Xiao, G. Zhang, R. Ma, X. Lu, C. Zhan, M. Zhang, A nonfullerene acceptor with a 1000 nm absorption edge enables ternary organic solar cells with improved optical and morphological properties and efficiencies over 15, *Energy Environ. Sci.* 12 (2019) 2529–2536.
- [42] L. Zhang, N. Yi, W. Zhou, Z. Yu, F. Liu, Y. Chen, Miscibility tuning for optimizing phase separation and vertical distribution toward highly efficient organic solar cells, *Adv. Sci.* 6 (2019), 1900565.
- [43] H. Xia, Y. Zhang, W. Deng, K. Liu, X. Xia, C.J. Su, U.S. Jeng, M. Zhang, J. Huang, J. Huang, Novel oligomer enables green solvent processed 17.5% ternary organic solar cells: synergistic energy loss reduction and morphology fine-tuning, *Adv. Mater.* (2022), 2107659.
- [44] L. Huang, G. Wang, W. Zhou, B. Fu, X. Cheng, L. Zhang, Z. Yuan, S. Xiong, L. Zhang, Y. Xie, Vertical stratification engineering for organic bulk-heterojunction devices, *ACS Nano* 12 (2018) 4440–4452.
- [45] Y. Pan, X. Zheng, J. Guo, Z. Chen, S. Li, C. He, S. Ye, X. Xia, S. Wang, X. Lu, A new end group on nonfullerene acceptors endows efficient organic solar cells with low energy losses, *Adv. Funct. Mater.* 32 (2021), 2108614.
- [46] Y. Xie, F. Yang, Y. Li, M.A. Uddin, P. Bi, B. Fan, Y. Cai, X. Hao, H.Y. Woo, W. Li, Morphology control enables efficient ternary organic solar cells, *Adv. Mater.* 30 (2018), 1803045.
- [47] S. Huang, Z. Huai, J. Ren, Y. Sun, X. Zhao, L. Wang, W. Kong, G. Fu, S. Yang, Improved morphology and interfacial contact of PBDB-T: N2200-based all-polymer solar cells by using the solvent additive p-anisaldehyde, *ACS Appl. Energy Mater.* 3 (2019) 358–365.